Interaction of Oligonucleotides with Gold Nanoparticles: Factors Beyond Electrostatic and Van-Der Waals Forces

(Article begins on next page)

Interaction of Oligonucleotides with Gold Nanoparticles: Factors Beyond Electrostatic and Van-Der Waals Forces

Shaila Thakur, Nicola Cavallini, Debora Ferrari, and Laura Fabris*

Motivated by the development of direct SERS for the detection of oligonucleotides as disease biomarkers, fundamental study is conducted for the adsorption of short model oligonucleotides onto gold nanoparticles (GNPs). It is observed that the variation in solution conditions has a profound effect on the way in which oligonucleotides bind to GNPs. The binding phenomenon is hypothesized to be a contribution of several factors: base composition, strand directionality, competition of oligonucleotides to bind to GNPs or undergo inter-strand assembly, among others. In addition to these factors, the properties of the individual bases in the given solution conditions (such as protonation or deprotonation) also affect the way in which the oligonucleotide strand binds to GNPs. In future, using this understanding could aid in developing direct SERS-based sensing methods for disease detection through identification of mutations in genetic biomarkers of disease. Based on the present hypothesis, knowledge gaps to fill and future research directions are suggested, to better understand these adsorption processes and optimize direct SERS biosensing.

1. Introduction

The recent years have witnessed a significant boost in the application of nucleotide-conjugated gold nanoparticles (GNPs).[1–4] Following the pioneering work of Mirkin et al.,[5] researchers have opened a plethora of avenues where the nucleotide-conjugated GNPs can be applied, with the majority of applications in biosensing and drug delivery.[6–12] Therefore, it is crucial to understand the factors that play a role in the binding of nucleotides to gold nanoparticles and to identify the best ways to achieve the bioconjugation without disturbing colloidal stability of GNPs. Researchers have identified different strategies to non-covalently bind nucleotides to GNPs and result in a stable suspension for biosensing. Some of these techniques include the low pH

method,[13–16] the freezing method,[17–22] the microwave heating-assisted conjugation,[23] the addition of salt,[24,25] and the dehydration methods,[26] among others. However, in most of the reported studies, the focus of the research has been on maximizing the loading of nucleotides on GNPs and very little emphasis has been placed on mechanistic details that may affect the binding process. Similarly, there is a great deal of information on the conformation of bare nucleotides at different solvent conditions, but the conformation of nucleotides in conjugation with GNPs at varying solution conditions is not well understood. As a result, there is a huge gap in interpreting the changes that occur when these nucleotides bind to GNPs under varied conditions. In fact, some of the most interesting phenomena, such as the formation of supra-molecular assemblies, arise from non-covalent interactions of very small nucleotides and metals/metal ions and this has been a topic of great interest in the scientific community.[27]

Some of the earlier studies provide us with useful insights about the study of stacking phenomena of short oligonucleotides (di- and trinucleotides) by observing changes in the UV–vis absorbance spectra.[28,29] There are studies on self-assembly of nucleotides (protonated, de-protonated, etc.) among themselves but less is known about the oligonucleotide structures formed in the presence of GNPs.[30–32] Thus, we aim to contribute in bridging this gap by providing useful insights into the role of 1) base homogeneity, 2) strand directionality, and 3) base-stacking of nucleotides in presence of GNPs. We have utilized the known fundamental concepts of interaction of nucleobases with gold nanoparticles and their affinity order to complement and extend our hypothesis of modes of interaction.[33–37] We try to provide a set of guidelines to the researchers regarding the suitability of binding conditions for customized applications.

We are mainly interested in the application of direct surface enhanced Raman spectroscopy (SERS) for the detection of mutations in nucleotide sequences as a prediction of diseases such as cancer. Thus, the main motivation for this work arises from the fact that the way in which nucleotides interact and conform around the nanoparticles determines their ability to be detected via SERS. For this study, we chose short 3-mer oligos as model systems because longer chains are known to exhibit significant folding and self-assembly and pose a greater steric hindrance

S. Thakur, N. Cavallini, D. Ferrari, L. Fabris
Department of Applied Science and Technology
Politecnico di Torino
Corso Duca degli Abruzzi 24, Turin 10129, Italy
E-mail: laura.fabris@polito.it

The ORCID identification number(s) for the author(s) of this article can be found under https://doi.org/10.1002/admi.202400067

**ADVANCED
SCIENCE NEWS**

www.advancedsciencenews.com

**ADVANCED
MATERIALS
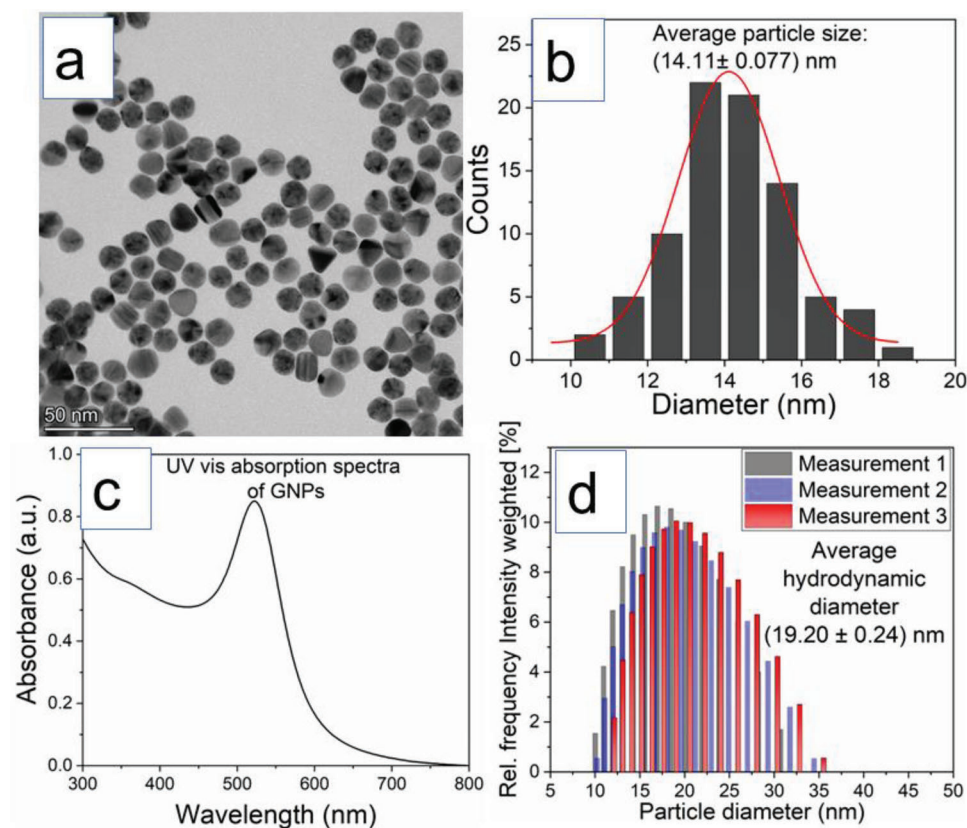INTERFACES**
Open Access

www.advmatinterfaces.de

Figure 1. Characterization of citrate stabilized GNPs a) TEM image showing well-dispersed spherical nanoparticles b) Size distribution of GNPs from the TEM image analyzed by ImageJ software c) UV–vis spectrum with GNPs plasmon band at 522 nm d) Particle size distribution (DLS) of GNPs showing an average hydrodynamic diameter of 19 nm.

towards non-covalent interaction with GNPs, thus complicating the fundamental understanding of the binding process. Although we do observe stacking interactions in small 3-mer oligos as well, we hypothesize that it is easier to unravel the dynamics of self-assembly and binding of small oligos to GNPs to begin with, dedicating our future work to the understanding of the interactions of GNPs with longer sequences.

In this work, we study the interaction of short trinucleotides with GNPs under different conditions of pH, temperature, and ionic strength. We also study the time-dependent kinetics of these interactions. We hope that this work can provide useful insight in the design of probes for DNA detection, in metal ion and small molecule sensing, and in drug delivery by easing the cellular internalization of GNPs.

2. Results and Discussion

2.1. Characterization of GNPs

Basic characterization results of GNPs are reported in **Figure 1**. The TEM image shown in Figure 1a depicts well-dispersed spherical gold nanoparticles with an average particle diameter of (14.11 ± 0.07) nm (analyzed by ImageJ, Figure 1b). The UV–vis absorption spectrum of GNPs in Figure 1c shows a plasmon band at 522 nm, which is a characteristic of GNPs of similar sizes.[38] The hydrodynamic diameter, as obtained by DLS, was reported to be

(19.20 ± 0.24) nm with an average polydispersity index of 9.46% (Figure 1d).

2.2. Choice of Experimental Conditions for Interaction of Oligonucleotides with GNPs

Since the binding of oligonucleotides to GNPs takes place through the electron-rich groups, the pH of the medium in which the interaction takes place is thought to have a significant effect on the binding. Similarly, temperature and salt concentration in the solution influence the interactions because these conditions dictate how freely the oligonucleotide chains move in the solution, ultimately influencing their orientation on the GNP surface. The interaction of individual nucleosides with GNPs has long been explored using different techniques.[35,39,40] An understanding of individual nucleobases interacting with GNPs can be applied to nucleotides since the primary interaction with the GNP surface takes place through the base moiety. It is also known that the nucleotide bases are hydrophilic in the order cytosine > guanine> thymine> adenine while the pentose sugar and phosphate moiety are more hydrophilic compared to the nucleobases.[41] Thus, a hydrophilic force of attraction between GNPs and the oligonucleotides must exist in neutral pH and room temperature conditions. For this reason, we chose to vary the pH and ionic strength of the medium to understand the

**ADVANCED
SCIENCE NEWS**

www.advancedsciencenews.com

**ADVANCED
MATERIALS
INTERFACES**
Open Access

www.advmatinterfaces.de

interplay of these forces in the binding phenomena. The atomic numbering of purine and pyrimidine rings has been included in the Supporting Information (Figure S1, Supporting Information) to aid the understanding of the interaction of individual atoms of the purine and pyrimidine ring with GNPs.

The choice of using UV–vis spectrophotometry for our study stems from the simplicity of this technique and the fact that the base interactions, stacking and self-assembly of the nucleotides can be derived from the shifts in the UV–vis spectra of the nucleotides.[32,42–45] With this study, we hope to establish a groundwork for the study of orientation of nucleotides on SERS substrates for biosensing.

It is worth pointing out that we noticed changes in the shape of oligonucleotide absorption spectra in the far UV region with solution conditions and on binding to GNPs (Figure S2, Supporting Information). There is an early study reporting the absorption of nucleotides in the far ultraviolet, but no recent reports addressing this behavior.[46] We aim to conduct future studies to explore this behaviour with the help of SERS.

2.3. Interaction of GNPs with Oligonucleotides of Similar Base Composition

For the ease of interpretation, we define a few terms related to the changes in UV–vis absorbance spectra of compounds that will be discussed in the subsequent sections. An increase in absorbance is termed as 'hyperchromic' while a decrease in absorbance is called 'hypochromic'. A shift of peak to lower wavelengths is referred to as 'hypsochromic' (i.e., 'blue shift'), whereas a peakshift to longer wavelengths is called 'bathochromic' (i.e., 'red shift'). A summary of the peak shifts is presented in Figure S3 (Supporting Information). **Figure 2** reports the UV-vis spectra obtained at varying pH, temperature, and ionic strength for homotrinucleotides of all nucleobases. As seen from Figure 2a, binding of AAA with GNPs at pH 3 is accompanied by a bathochromic shift with negligible change in the magnitude of absorbance indicating interactions between positively charged protonated bases of AAA (protonated N1 endocyclic nitrogen atom) with the negatively charged gold nanoparticles. The N—H●●●N H bonds between individual adenine bases in AAA are broken upon protonation and the instability of electrons caused by broken H bonds is counterbalanced by the partial π-π interactions between the adenine groups.[47] Hyperchromic shift at pH 6 and 9 indicates binding of AAA with GNPs mainly through Van der Waals forces. The lack of deprotonation of AAA at pH 9 (pKa for adenine is 9.8) makes the interactions similar to that at neutral pH, despite the fact that the electrostatic repulsion between AAA and GNPs may increase at pH 9.[48] In addition, there is also a role played by Na$^+$ ions at higher pH in the charge neutralization of citrate ions on the surface of GNPs, although this may be less significant. We would like to make a point about the low pH conditions that in addition to the nitrogen-containing functional groups, the phosphates, more specifically the oxygen carrying a negative charge associated with the phosphate (oxygen anion (pKa≈6.3),[49] are also protonated at pH 3 bringing the phosphate group a greater ability to bind to GNPs than at neutral or alkaline pH. As a result, we believe that protonated AAA form regular structures with GNPs, as shown in Figure S4 (Supporting Information).

The behavior is different when AAA binds to GNPs at different temperatures. Hypochromic and bathochromic shifts in Figure 2b indicate that AAA forms duplex structures on freezing with GNPs at -20°C. According to previous reports by Liu et al.,[17] the oligonucleotides are "aligned and stretched" in the frozen state and these stretched oligonucleotides bind perpendicular to the surface of GNPs. It has been observed that when the GNPs-oligonucleotide solution freezes, the conjugate remains trapped in the spaces between the ice network due to the partial hydrophobicity of oligonucleotides so that the stretched oligonucleotides bind to GNPs in this restricted environment, possibly leading to a stronger interaction.[17,18] We would like to point out that the temperature control experiments were carried out with incubation of oligonucleotides in as-synthesized citrate stabilized GNPs, in contrast to the pH and NaCl concentration studies (which were carried out with GNPs pellet resuspended in water). This is because of better stability of as-synthesized citrate capped GNPs with oligonucleotides at low temperatures compared to the ones that were re-suspended in water. Thus, apart from the effects introduced by temperature, presence of citrate might also play a role in the interaction of GNPs with oligonucleotides at low temperature. At higher concentrations of NaCl (10 mM and 30 mM), the spectra of AAA exhibited changes in intensity with no evident shift in peak position (Figure 2c). At lower concentration of NaCl (1 mM), the oligonucleotides stiffen and the interaction of AAA at low ionic strength manifests itself as a hyperchromic and bathochromic shift. A coating corona of AAA on GNPs has been shown in the TEM images of Figure S5 (Supporting Information).

CCC was found to bind differently to GNPs compared to AAA (Figure 2d–f). The protonation and deprotonation sites for cytosine are N3 (pKa: 4.6) and N1 (pKa: 12.2), respectively. Stacking of 'bare' protonated and semi-protonated CCC at pH 3 can be seen from the spectral shifts in Figure 2d. A large bathochromic and hypochromic shift in the UV-vis spectra is consistent with the behavior of protonated/semi-protonated cytosine assembly.[50,51] In contrast to AAA, CCC exhibits hypsochromism on binding to GNPs at pH 6 and 9. Large hypsochromic and hyperchromic shifts in the spectra of CCC were also seen upon interaction with GNPs at pH 9. Similar shifts were observed when CCC interacts with GNPs at low temperatures and different NaCl concentrations (Figure 2e,f). Previous reports indicate that a hypsochromic shift accompanied by a hyperchromic shift in the spectra of DNA might be indicative of a strong intercalative binding.[52] While it is difficult to explain the intercalation of GNPs with short oligonucleotides, it is possible that CCC strands stack together trapping GNPs between the adjacent bases of the oligonucleotide assembly giving rise to noticeable hypsochromic shifts.

Guanine-containing oligonucleotides are known for their complexity, as they form a wide variety of secondary structures under different conditions.[31,53] At pH 3 and 9, strands of bare GGG assembled together (evidenced by hypochromic and bathochromic shifts in Figure 2g) but in presence of GNPs, the N(7) and C6 = O6 carbonyl group of guanine bind to GNPs and lead to the dissociation of the assembled structure (noted by large bathochromic and hyperchromic shift) at pH 3 and 9. The deprotonated GGG (at N1 site) causes a larger hyperchromic effect when bound to gold nanoparticles compared to protonated GGG (at N7 site). To summarize, assemblies of bare GGG break when combined with
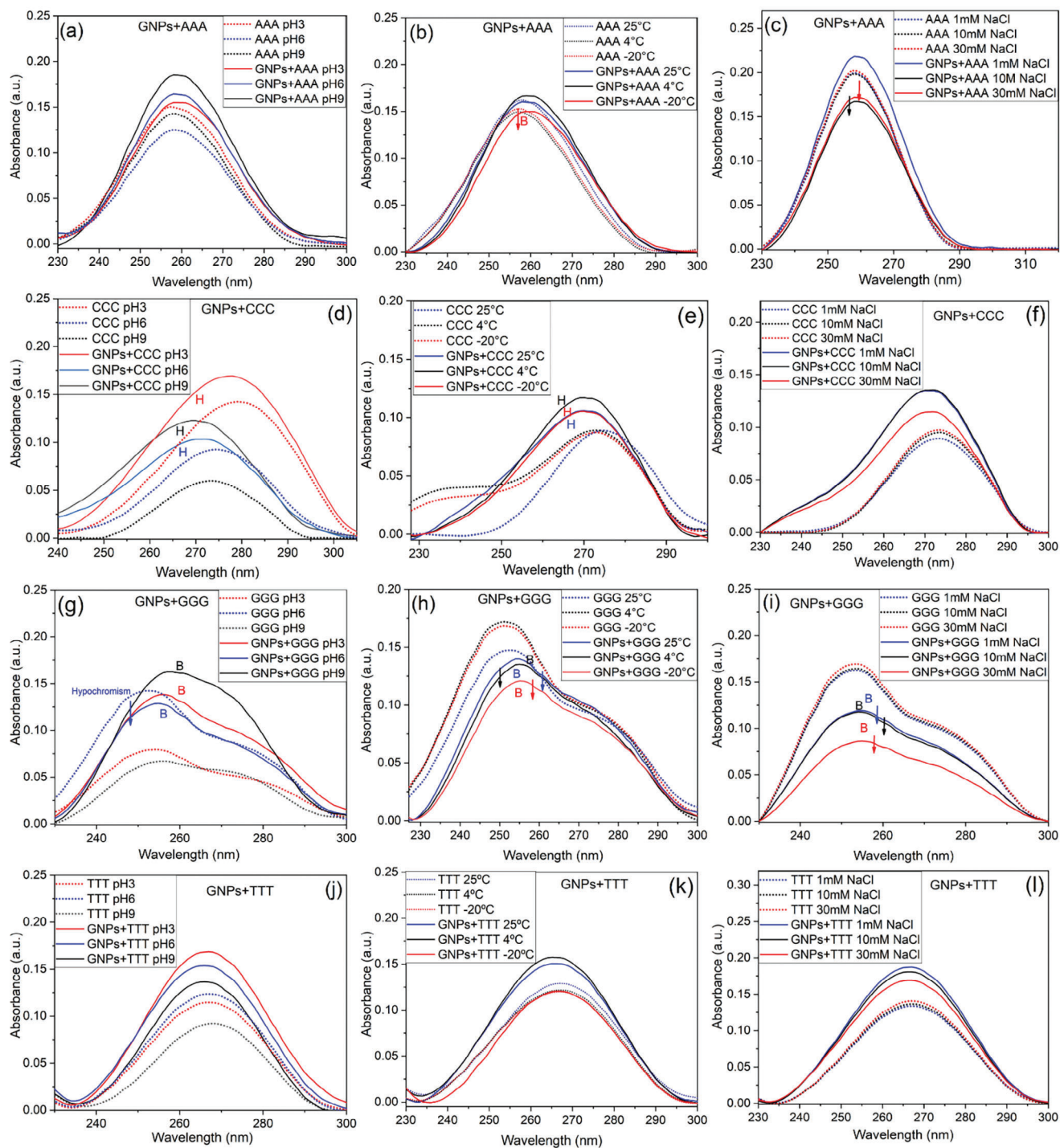
2400067 (3 of 13)

ADVANCED
SCIENCE NEWS

www.advancedsciencenews.com

ADVANCED
MATERIALS
INTERFACES
Open Access

www.advmatinterfaces.de

Figure 2. UV vis absorption spectra of oligonucleotides with similar base composition a–c) AAA d–f) CCC g–i) GGG j–l) TTT, at variable pH (3, 6, 9) (a, d, f, i), temperature (25 °C, 4 °C, -20 °C) (b, e, g, j) and NaCl concentration (1 mM, 10 mM, 30 mM) (c, f, h, k). The arrows pointing downwards indicate hypochromism, the letter 'B' stands for bathochromism (red shift) while 'H' stands for hypsochromism (blue shift). It can be noted that only CCC exhibits hypsochromism while only GGG shows a change in spectral shape in addition to changes in peak position and intensity.

**ADVANCED
SCIENCE NEWS**

www.advancedsciencenews.com

**ADVANCED
MATERIALS
INTERFACES**

www.advmatinterfaces.de

GNPs, as there is a competition between the interaction of guanine strands with each other and with GNPs. Additionally, the change in shape of the guanine spectra (especially at pH 9) is indicative of a greater change in the structure of GGG than just re-distribution of electrons along the purine ring; thus, further studies are needed to address this behavior. Similar assemblies of GGG strands formed when they were incubated at low temperatures (Figure 2h) (large hypochromic and bathochromic shift) and at 30 mM NaCl concentration (Figure 2i).

Thymine is not protonated at the studied acidity (pKa for thymine is less than 2) thus the binding of TTT with GNPs at pH 3 is possibly due to the displacement of citrate ions by H$^+$, which facilitates the interaction of C4 = O4 of the pyrimidine ring with the surface of GNPs.[54] The association of TTT with GNPs at other pH conditions is manifested as an increase in intensity with no visible spectral shifts, as shown in Figure 2j, which agrees with reported literature for thymine interactions with GNPs.[55] However, at pH 9, hypsochromic and hyperchromic shifts indicate interaction of partially deprotonated thymine (pKa: 9.8) with GNPs. A high hypsochromic and hyperchromic shift of TTT in association with as-synthesized GNPs at room temperature emphasizes the role played by citrate ions in the binding process (Figure 2k). The interaction of TTT with GNPs at different NaCl concentrations was characterized by hyperchromicity of the peaks (Figure 2l).

2.4. Base Position (directionality)-Dependent Association of Oligonucleotides with GNPs

The substitution of adenine with thymine at different positions in the AAA strand alters the interaction with GNPs. Substitution of adenine with thymine at the 5' and 3' ends of AAA (TAA (5') and AAT (3')) gives rise to a 'directionality' of the strand. The way in which all the bases are linked together in a nucleotide imparts polarity to the strand with a 5' end presenting a protruding phosphate and 3' end containing an exposed hydroxyl group.[56]

The changes in spectra of TAA, AAT, and ATA and a scheme of their interaction with GNPs are presented in **Figure 3**. Figure 3a shows that at pH 6, the interaction of TAA with GNPs results in hypochromic and bathochromic shift possibly because the 3' adenine in TAA can form canonical Watson-Crick base pair with the 5' thymine of adjacent strand. On the other hand, we find that the protonation (pH 3) and deprotonation (pH 9) of adenine in TAA hinders the inter-strand stacking (hyperchromic shift) of TAA while interacting with GNPs (bathochromic shift). This phenomenon was not observed for AAT binding to GNPs at pH 6 mostly because in AAT the presence of bulky phosphate groups with adenine poses a greater steric hindrance towards pairing compared to TAA. At pH 3, the absorbance of bare AAT and TAA is seen to reduce, indicating inter-strand interactions due to base protonation. Additionally, because of the inability of thymine to be protonated at pH 3, we hypothesize that the spectral differences observed for 5'-TAA-3' and 5'-AAT-3' at pH 3 (larger hypochromism for TAA than AAT) are solely governed by the protonation of adenine in the oligonucleotide chain. Protonation of the terminal phosphate at the 5' end of TAA is easier compared to that in AAT because adenine at the 5' end competes with the 5' phosphate for the protons. Thus, in addition

to adenine, 5' phosphates are also protonated in TAA, which allows them to come closer to each other and stack with adjacent strands leading to a more compact structure than in AAT. This phenomenon may also explain the negligible change in the spectra of AAT and GNP-AAT at pH 3 while a large increase in intensity for GNP-TAA, as shown in Figure 3a,d. It is also worth noting that AAA showed higher spectral shifts when bound to GNPs at pH 3 and 9 compared to AAT and TAA. In case of AAT and TAA, the adenine present at the end of the chain is protonated or de-protonated depending on the pH. The middle adenine in AAT and TAA is joined by thymine at one end and by the protonated/de-protonated adenine at the other end. The protonation/deprotonation of the middle adenine may be inhibited or slowed down (compared to AAA) due to the steric hindrance caused by thymine at the terminal that stays neutral at the studied pH conditions.[57]

By varying the temperatures, we observe that TAA still undergoes stacking with other strands while simultaneously interacting with GNPs at 25 °C and also at freezing conditions (-20°C) (Figure 3b), while we only observe stacking of AAT while interacting with GNPs at -20°C and not at 25 °C. At 4 °C, hyperchromic and bathochromic shift is observed for both TAA and AAT interacting with GNPs. Thus, it's not just temperature reduction but the process of freezing that causes these oligonucleotide strands to stack and form clusters of GNPs. It can be proposed that citrate ions hinder the accessibility of 5' adenine in AAT due to electrostatic repulsion with the protruding 5' phosphate group. Thus, both the 5' adenine and the 3' thymine of AAT are less likely to interact with the adjacent strands as well as with the GNPs. In case of TAA, the citrate ions hinder the accessibility of the 5' thymine but the the 3' adenine can still interact with GNPs and with the adjacent TAA strands. This interaction manifests itself as hypochromic spectral shift.

At different NaCl concentrations (Figure 3c,f), the binding of AAT and TAA is similar and can be accounted by the fact that higher salt concentration (30 mM) leads to the compaction of oligonucleotide chains which in turn makes them more likely to self-assemble. This behavior is shown by the hypochromic and bathochromic shift in the spectra of GNPs-AAT (Figure 3c) and GNPs-TAA (Figure 3f). The stacking of oligonucleotide chains, increased at higher NaCl concentration mainly due to the Na+, lowers the electrostatic repulsion between the phosphodiester backbones and eases the interaction of adjacent chains. These observations led us to hypothesize that directionality plays a critical role in the binding process at certain conditions as described above, and further studies can be conducted with longer oligonucleotides and other techniques (such as SERS) to describe this phenomenon better.

Similar to bare AAT and TAA, bare ATA strands stack with each other at pH 3 and 9 (Figure 3g). However, the assembled structures disintegrate when bound to GNPs, as evident from the increased spectral intensity. We make a reasoning based on the competition of oligonucleotides to form canonical base pairs or bind to GNPs. Researchers have reported that polyA prefers the gold surface more than the complementary polyT in the same media because the attractive forces between gold and adenine overcome the binding energy of polyA-polyT duplexes resulting in the separation of polyA from the duplex to bind to gold (denaturation of the duplex).[58] This preference might explain the
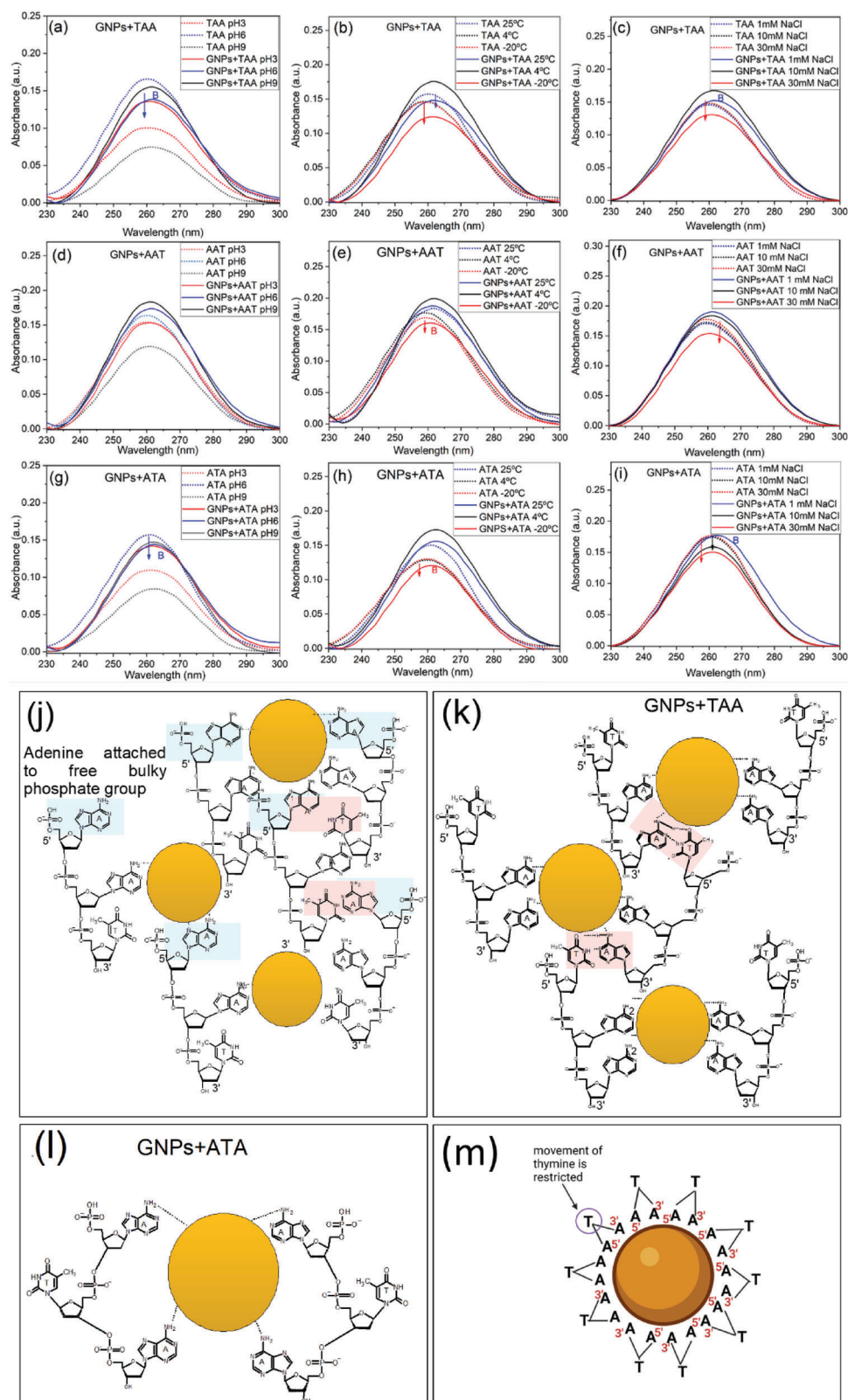
**ADVANCED
SCIENCE NEWS**

www.advancedsciencenews.com

**ADVANCED
MATERIALS
INTERFACES**
Open Access

www.advmatinterfaces.de

Figure 3. UV–vis absorbance spectra of TAA a–c), AAT d–f) and ATA g–i) at different conditions of pH (3, 6, 9) (a, d, g), temperature (25 °C, 4 °C, -20 °C) (b, e, h), and NaCl concentration (1 mM, 10 mM, 30 mM) (c, f, i). j, k) Schematic of interaction of GNPs with AAT (j) and TAA (k) indicating the ease of stacking of TAA chains compared to AAT due to steric hindrance. l, m) Schematic of orientation of ATA around GNPs. We propose that ATA adapts an inverse V conformation on GNPs surface.

**ADVANCED
SCIENCE NEWS**

www.advancedsciencenews.com

**ADVANCED
MATERIALS
INTERFACES**

Open Access

www.advmatinterfaces.de

fact that in the absence of GNPs, A- and T-containing oligonucleotides tend to stack through the canonical A—T interactions but disassemble in the presence of GNPs. This theory does not hold true under all the solution conditions, and we do observe stacked structures of ATA even after binding to GNPs at neutral pH conditions. Another interesting observation in the spectra of GNPs-ATA at different pH is that they overlap. Overlapping spectra might indicate that the orientation of ATA on GNPs is similar at acidic, basic, and neutral conditions. We hypothesize that ATA adapts an inverse 'V' orientation on GNPs with the two terminal adenines bound to the surface and thymine pointed outwards, as shown in Figure 3l,m. The reason for this depiction is based on the higher affinity of adenine to the gold surface compared to that of thymine and the fact that thymine pointing upwards poses a greater steric hindrance for the protonation/deprotonation of bound adenines, rendering the spectra similar at acidic, neutral, and alkaline pH. Due to the inability of thymine to be protonated at pH 3,[59] and the fact that both adenine and thymine are not deprotonated at pH 9, the conformation of ATA on GNPs remains the same. It is worth mentioning that thymine is much less likely to interact with adenine of adjacent chains because it is bound by adenine molecules on both ends and is much more restricted compared to the thymine in AAT and TAA.

At different temperatures (Figure 3h), ATA showed similar hypochromic and bathochromic shift at -20 °C indicative of the stacking of stretched and aligned ATA (unlike the inverse V conformation) bound to GNPs with other free ATA strands. The spectrum for GNPs-ATA at 4 °C shows hyperchromic and bathochromic shifts representing binding of ATA with GNPs without stacking with adjacent strands.

While the studied oligonucleotides are very short in length, NaCl can still alter the binding ability of oligonucleotides significantly by altering its flexibility and the phosphorus-base distance.[60] GNPs-ATA showed a bathochromic shift with no change in peak intensity at 1mM NaCl concentration while GNPs-ATA exhibited a hypochromic shift with no change in peak position at 10 mM and 30 mM NaCl concentration (Figure 3i). This behavior is similar to other reports for nucleotides interacting with carbon nanotube surfaces at different concentrations of NaCl.[61] It has also been known that at lower concentration of NaCl, the oligonucleotide chain stiffens and spreads out on the interacting surface (in this case GNPs) while at higher salt concentrations, the oligonucleotide strands undergo self-stacking and form compact structures.[61] Apart from the conformation of oligonucleotide chains on GNPs, the grafting density might also be of interest. Thus, we calculated the number of oligonucleotide strands bound to GNPs (details can be found in Section S6 (Supporting Information) (Figure S6, Supporting Information)) and determined that incubation conditions such as pH 3, -20 °C and 30 mM NaCl mostly increase the number of oligonucleotide strands bound to GNPs (Figure S6, Supporting Information) compared to neutral pH, room temperature, and no salt.

2.5. Colloidal Stability of GNPs Bound to Oligonucleotides

The colloidal stability of GNPs is altered in the presence of oligonucleotides. Although there have been very detailed reports on the base composition-dependent effect of short oligonucleotides on the colloidal stability of GNPs, these studies mostly focused on the chemically modified oligonucleotides.[62,63] While it has been known that short sequences of oligonucleotides act as capping agents for GNPs and protect the colloid under extreme conditions, we observed that the capping effect is strongly dependent on the oligonucleotide base composition and interaction conditions.

It was found that the oligonucleotides with similar bases are more efficient in capping the colloidal GNPs at conditions where bare GNPs aggregate, such as low temperature, acidic pH, and high salt concentrations. The color of GNP solution changes depending on the oligonucleotide sequence, as shown in Figure S7 (Supporting Information). The oligonucleotides AAA, CCC, GGG, and TTT protect the GNPs from aggregating under extreme conditions of temperature and salt concentration (-20 °C and 30 mM NaCl) (Figure S8, Supporting Information). On the contrary, oligonucleotides AAT, TAA, and ATA were not as effective as capping agents and their interaction with GNPs at pH 3, -20 °C and high salt concentrations led to aggregation, (Figure S9, Supporting Information). This is likely due to the inter-strand A-T interactions that bring the GNPs close together (as mentioned before) leading to their collapse under harsh solution conditions. The red shifts observed in the spectra are due to the coupling of plasmonic oscillations from individual gold nanoparticles as they assemble.[21] Future possibilities exist in probing the SERS activity of GNPs assemblies formed by oligonucleotides at these conditions for biosensing.

We would like to point out that there is a difference between complete aggregation and assemblies of GNPs that still maintain their colloidal stability. For instance, as shown in Figure 4, the particle size distribution for oligonucleotides of similar base composition (obtained by DLS) bound to GNPs is higher at extreme conditions of pH, temperature, and NaCl concentration but the GNPs still maintain their colloidal stability and display a sharp plasmon band, unlike for the aggregated GNPs for which the localized surface plasmon resonance (LSPR) band is flat and shifted to even higher wavelengths (Figure S8, Supporting Information). The presence of small clusters of GNPs are evident in the TEM images shown in **Figures 4** and S10 (Supporting Information) when GNPs are associated with oligonucleotides of similar base composition but aggregation can be seen in the presence of oligonucleotides of dissimilar base composition. The increase of NaCl concentration to 30 mM leads to aggregation of GNPs as a result of short-range London forces.[64] The homo-oligonucleotides protect the GNPs at high concentration of NaCl by electrostatic repulsion due to the phosphate backbone of oligonucleotides. It can be inferred that the charge neutralization of phosphate groups of homo-oligonucleotides is not sufficient to cause GNP aggregation as the repulsive forces of similar bases along the strand are sufficient to keep the GNPs suspended in the colloid. However, due to dissimilar bases in the oligonucleotide chain in case of ATA, TAA, and AAT, the protonation of phosphate groups at low pH disrupts the electrostatic forces of repulsion enough to disturb the stability of the colloid and cause aggregation.[65] The particle size distribution of GNPs at different conditions in shown in Figure S11 (Supporting Information). The zeta potential values for GNPs-oligonucleotide conjugates at different conditions (Figure S12, Supporting Information) give an indication of the colloidal stability of GNPs-oligonucleotide
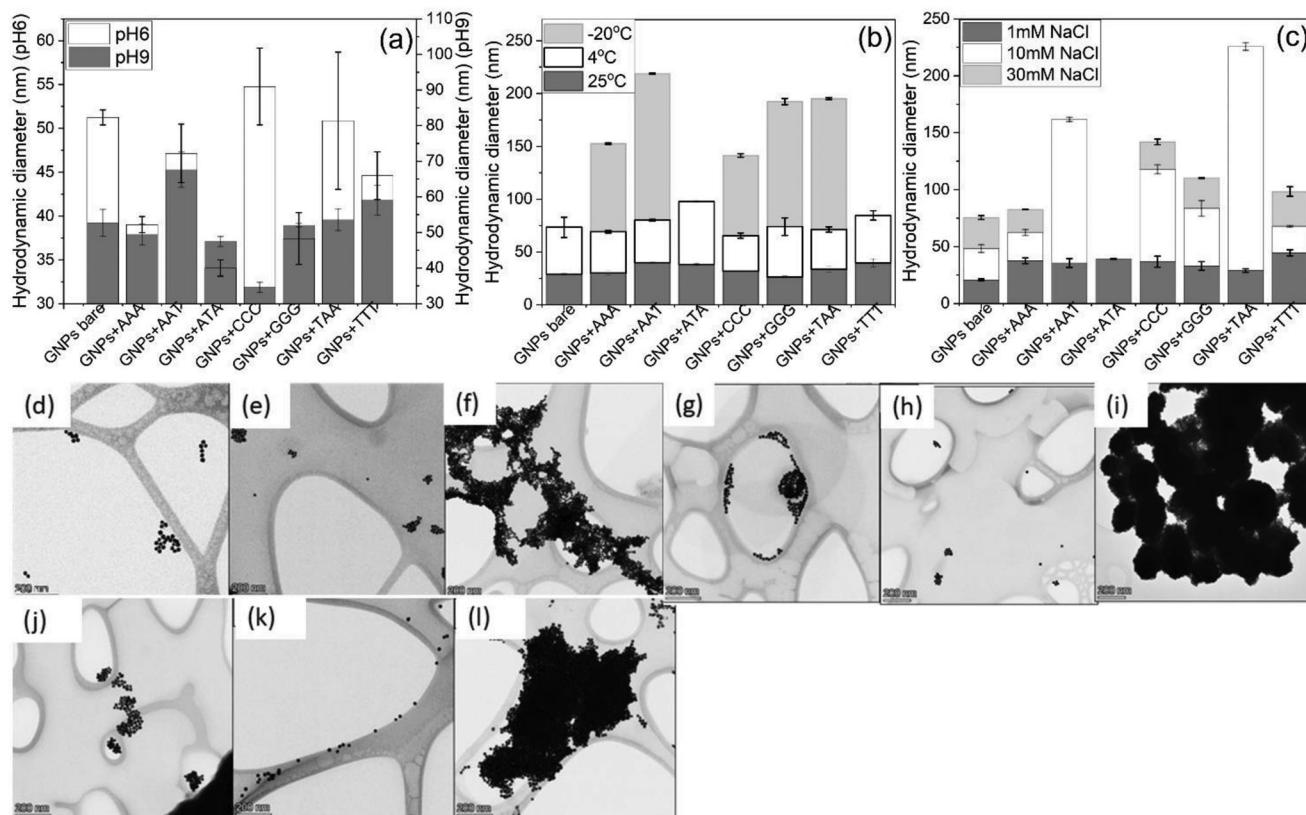
ADVANCED
SCIENCE NEWS

www.advancedsciencenews.com

ADVANCED
MATERIALS
INTERFACES

www.advmatinterfaces.de

Figure 4. Change in the size of GNPs on binding to oligonucleotides of different composition at a) pH 3, 6 and 9 b) temperatures 25°C, 4°C and -20°C, and c) NaCl concentration 1 mM, 10 mM and 30 mM. TEM images of d, g, j) GNPs+AAA (e, h, k) GNPs+ GGG f, I, l) GNPs+ATA at different conditions (d–f) pH 3 (g–i) -20°C (j–l) 30mM NaCl. The GNPs protected from harsh conditions of pH, temperature and salt concentration by AAA and GGG (and other oligonucleotides of similar base composition as shown in Figure S10, Supporting Information) but aggregate with TAA (and other oligonucleotides of dissimilar base composition). Note that the aggregated nanoparticles (particle size > 500 nm) have not been considered for the DLS measurements as these particles settled down at the bottom of the cuvette during measurements.

conjugates. Interestingly, it appears that, under the 200 V needed to carry out the measurement, the GNP-oligonucleotide conjugates experience varying degrees of instability, even when the system is left undisturbed, indicating that, under strong chemisorption conditions, these conjugates are extremely sensitive to applied electric fields.

2.6. Kinetics of Binding of Oligonucleotides to GNPs

A time-dependent study of the interaction of oligonucleotides with GNPs from the first instance of addition showed that, in some cases, the association phenomenon is faster in the beginning and then slows down afterwards due to GNPs surface saturation. For some other oligonucleotides, the association process was slower and almost constant throughout the studied time-frame. The kinetic spectra of association of oligonucleotides with GNPs have been reported in the Supporting Information (Figure S13, Supporting Information).

Due to the intricacies involved in the interpretation of kinetic spectral profiles, we employed a multivariate curve resolution (MCR) to deconvolute the spectral overlap for each component that appears and disappears during the binding process. We selected a 3-component model based on the reasoning that

three species must be present in the system i.e. GNPs, oligonucleotides, and GNPs-oligonucleotide conjugate. Additionally, the spectra extracted by the MCR algorithm were rather similar to their actual counterparts as measured by UV–vis spectrophotometer (Figure S14, Supporting Information), thus confirming the matching of the chemical species with the modelled MCR components. **Figure 5** shows the resolved concentration of each species with time as extracted by the MCR algorithm.

The GNPs+oligonucleotides combinations that did not show indications of stacking (based on the known tendency of bases to stack together and hypochromic and bathochromic shift in the spectra) were modelled by a 3-component model (AAA, AAT, ATA, TTT). We used a 4-component model for systems that showed a tendency to form aggregates (Figure S15, Supporting Information).

The concentration of GNPs-AAA increases over time (blue line), more rapidly after 10 minutes, while free AAA (red line) and free GNP concentration (yellow line) exhibit a marked decline in concentration proportionally after around 10 minutes (Figure 5a). The transition point of 10 minutes marks the starting of accelerated association of AAA with GNPs.

The spectral changes in AAT on association with GNPs is more rapid and a maximum shift of 5 nm at t = 0 min indicates instantaneous adsorption (Figure 5b). The shifts decreased at longer
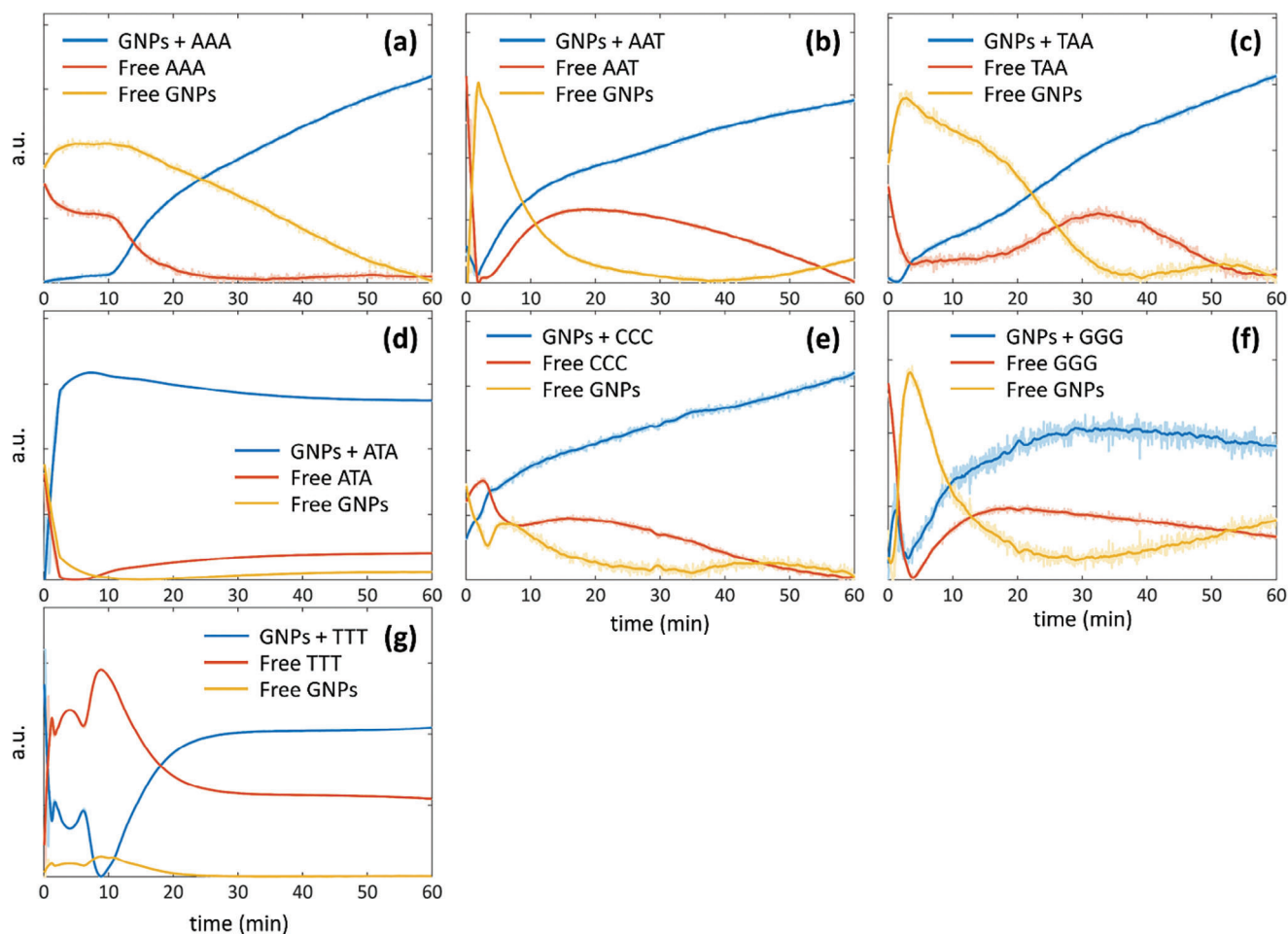
**ADVANCED
SCIENCE NEWS**

www.advancedsciencenews.com

**ADVANCED
MATERIALS
INTERFACES**
Open Access

www.advmatinterfaces.de

Figure 5. Resolved 3-component concentration profiles (preprocessing: SNV+offset) obtained after MCR data analysis for the UV vis absorbance kinetic profiles of binding of different oligonucleotides with GNPs for 60 minutes a) GNPs+AAA b) GNPs+AAT c) GNPs+TAA d) GNPs+ATA e) GNPs+CCC f) GNPs+GGG g) GNPs+TTT.

durations, similar to what observed for other oligonucleotides. At t = 2 min, a rapid decline in the free AAT concentration (red line) and rapid increase in GNPs concentration (yellow line) are observed. A decrease in AAT concentration without the formation of conjugates indicates stacking of AAT with each other. At this stage, AAT strands prefer to stack with each other rather than forming conjugates with GNPs. After t = 2 min, the AAT unstacks and binds to GNPs. While some of the strands bind to GNPs, the others remain free in the solution. Over time, the concentration trends indicate gradual dissociation of the conjugate.

For GNPs+TAA, the resolved profiles are similar to GNPs+AAT (Figure 5c). Until t = 1 min, no conjugate is formed despite the decrease in free TAA concentration, which is followed by unstacking and association of individual strands with GNPs. The presence of a hump in the spectra of free TAA after 30 minutes indicates that TAA dissociates and is released as free TAA. It is unlikely that TAA dissociates from the GNPs+TAA conjugate because of the fact that the conjugate concentration still increases, and free GNPs reduce after 30 minutes. Thus, the only way that free TAA concentration rises suddenly is by the dissociation of stacked TAA assemblies. This behavior is

more clearly depicted by the 4-component system presented in the Supplementary Information (Figure S15a, Supporting Information). The major difference shows up in the initial 2 minutes and later stages.

The MCR-resolved concentration profiles of the 3-component model for GNPs association with ATA are shown in Figure 5d. An initial rapid binding of ATA with GNPs is indicated by a rise in GNPs+ATA concentration (blue line), and a proportional decline in free GNPs and ATA concentration. Some dissociation of ATA from GNPs over time is shown by a gradual downward trend for GNPs+ATA and a gradual upward trend for free GNPs and free ATA.

Figure 5e shows the MCR-resolved profiles for the kinetics of interaction of CCC with GNPs. Until t = 4 min, free GNPs concentration reduce and conjugate concentration increase (blue). However, the concentration of CCC goes down for a short while and then starts to reduce. To probe this behavior, we consider the four-component analysis of this system, shown in the Figure S15b (Supporting Information).

From Figure S15b (Supporting Information), we see that the conjugate concentration suddenly spikes up (blue) at t = 3 min.

**ADVANCED
SCIENCE NEWS**

www.advancedsciencenews.com

**ADVANCED
MATERIALS
INTERFACES**

www.advmatinterfaces.de

The changes that take place in the system for the first 3 minutes can be noted from the spectra of other species: the concentration of GNPs reduce, free CCC increases, and a third species is formed which is most likely the stacked CCC. It appears that the initial conjugates are formed with GNPs interacting with stacked CCC and then, as the CCC strands dissociate, some of them contribute to the free CCC and some to the formation of conjugates.

The resolved MCR kinetic profiles for GNPs+GGG are shown in Figure 5f. For GGG, in addition to a large spectral shift (around 13 nm), for the first instance of addition of GGG to GNPs (t = 0 min), it can also be noticed that the shoulder peak of GGG is almost absent when it comes in contact with GNPs, while it is seen to evolve over time becoming more prominent after overnight incubation (Figure 2l, solid blue curve). This behavior indicates a structural change in GGG and the formation of inter-strand assemblies that disintegrate over time as the strand interacts with GNPs. Further studies are needed to describe the structural change of GGG over time. The first region of changes in GGG indicate formation of GNPs+GGG (increase in solid blue line) and decrease in free GNPs (yellow line) and GGG (red line). The second region marks the dissociation of the GNPs+GGG conjugate, indicated by an increase in free GNPs (yellow line). Again, the concentration of free GGG still keeps on reducing, indicating the formation of assemblies of GGG rather than that of GNPs-GGG conjugates. At t = 4 min, the trend again reverses and GGG binds to GNPs rather than forming inter-strand assemblies, as evident by the increase in conjugate concentration and a reduction in free GNPs and GGG concentration. A 4-component resolved profiles for GNPs+GGG kinetics is shown in Figure S15c (Supporting Information). The spectrum of TTT changes rapidly on association with GNPs, which is likely due to the low affinity of thymine to GNPs (Figure 5g). The concentrations stabilize after 20 minutes and no association/dissociation of TTT from GNPs takes place after that.

These findings serve as important design considerations for applications such as biosensors where the detection of different nucleotide sequences is dependent on the time of interaction.

To summarize, the chemical mechanism of interaction of oligonucleotides with GNPs can be mainly explained by the base affinity and charge of oligonucleotides. Protonated oligonucleotides (at low pH) are more capable of forming hydrogen bonds than their neutral counterparts, thus exhibiting a stronger binding with GNPs. The base affinity for binding to GNPs is based on the ease of accessibility of electrons of the base (aromatic nitrogen, exocyclic amino and keto groups) to GNPs.[66] As already mentioned in section 2.3, adenine interacts with gold by the N6 (amino) and N7 (imino) groups; cytosine binds through the N3 and oxygen of the keto group (O2) in the purine ring; guanine binds through the N7 and O6 of pyrimidine ring while thymine binds by O4 (in close proximity to CH_3 group of the purine ring). For a more detailed explanation on the binding of bases and nucleotides to GNPs, the readers are invited to refer to excellent reviews on the interaction of GNPs with nucleotides.[67,68] As discussed earlier, the interactions are not solely GNPs+oligonucleotide but there are also inter-strand base-base interactions depending on the solution conditions and flexibility of the oligonucleotide chain (as in case of AAT, TAA and ATA).

3. Conclusion

GNPs-oligonucleotide conjugates have been used for the detection of pathogens by binding to complementary DNA inside cells, for the recognition of platelet-derived growth factors (anticoagulation), protein kinases and telomerases, for the detection of drugs (like cocaine) in body fluids, and so forth.[69] In addition to sensing, GNPs-DNA conjugates have also been studied as anti-coagulant drugs[70] and for the targeted treatment of cancer,[71,72] bacteria[73] and viruses.[74,75] We have explored some of the factors that have a direct effect on the binding of oligonucleotides with GNPs and compared the differences in interaction of oligonucleotides with GNPs at different conditions of pH, temperature and NaCl concentration. The ability of individual bases to be protonated/deprotonated governs the overall interaction of the oligonucleotide chain to GNPs. We also observed the differences in behavior on lowering the incubation temperature to 4 °C and freezing (-20 °C). We believe that the binding at -20 °C is mostly caused by the phase transition from liquid to solid and the restricted space of interaction of oligonucleotides with GNPs. We aim to conduct further studies to explore the binding at -20 °C by SERS. For different NaCl concentrations, we found that increasing the NaCl concentration to 30 mM gives rise to higher spectral shifts compared to lower concentrations indicating better binding at higher salt concentrations.

Under the studied conditions, we found some interesting observations that can be employed for designing a SERS based biosensor, which is dependent on the orientation of the target analyte on the substrates. Firstly, we found that the oligonucleotides with similar base composition (like AAA, CCC, GGG, TTT) are capable of protecting the colloidal stability of GNPs at extreme pH and temperature conditions (pH 3 and -20 °C) while oligonucleotides with dissimilar bases are unable to provide such effect. Secondly, we found that the directionality of strand plays an important role in the interaction of oligonucleotides with GNPs (TAA interacts differently with GNPs compared to AAT). Lastly, the spectral shifts arising from the interaction of oligonucleotides with GNPs initially (t = 0 min) may be very different from their behavior in stable conditions (overnight incubation). Thus, depending on the targeted application, one might prefer the time frame in which the oligonucleotides exhibit highest spectral shifts (indicating strong binding with GNPs) or wait for the time when there is negligible association/dissociation of oligonucleotides on GNPs (stable suspension). For drug delivery and nucleotide detection by probe hybridization, freezing conditions (-20 °C) might work well due to high DNA loading density (vertical orientation of oligonucleotides on GNPs) and accessibility of all the bases for hybridization. But for applications such as direct SERS-based biosensing, we would like the oligonucleotide chains to lay flat on the GNPs surface, and for this reason, low pH, neutral conditions (pH 6 and room temperature) and high salt concentration (30 mM NaCl) would work better. Experiments involving the combination of different solution conditions would be required to complement our present understanding of conformation of oligonucleotides on GNPs. Eventually, the nucleotide conformation on GNPs can be tailored to suit specific applications such as SERS based biosensing, which is the future goal of this research.

4. Experimental Section

Materials: Oligonucleotides, with sequences listed in the (Table S1, Supporting Information) were purchased from BioFab Research (Rome, Italy). The lyophilized oligonucleotide powder was resuspended in molecular biology grade water to obtain 100 μM stock solutions. Oligonucleotide concentration was determined by measuring the absorbance at 260 nm with molar extinction coefficients provided in the (Table S1, Supporting Information). Tetrachloroauric(III) acid trihydrate 99% ($HAuCl_4$), trisodium citrate ($Na_3C_6H_5O_7$), sodium chloride (NaCl), hydrochloric acid (HCl), and sodium hydroxide (NaOH) were obtained from Sigma-Aldrich, Europe.

Preparation of Gold Nanoparticles (GNPs): GNPs were synthesized by the standard Turkevich method.[76] Briefly, trisodium citrate solution (2.5 mM, 52.5 ml), preheated to reaction temperature, was quickly added to a boiling solution of $HAuCl_4$ solution (0.25 mM, 60 ml). The solution changed color from colorless to dark purple in 20 minutes and then to brilliant red in 45 minutes. The reaction was allowed to proceed for a total of 60 minutes, after which the solution was removed from stirring, cooled, and stored in glass vials covered with aluminium foil at room temperature for future use.

The morphology of GNPs was studied by Transmission Electron Microscopy (TEM) TALOS F200X, Thermo Scientific), equipped with a Field Emission Gun (FEG) emitter, operated at 200kV of accelerating voltage. Images were acquired in Bright-Field TEM mode by means of a 16Mpx CMOS camera (Ceta, Thermo Scientific), using a 30 micrometers objective aperture. Samples for TEM were prepared by drop casting 10 μL of dilute GNPs (10-fold dilution) on a continuous ultrathin carbon film-coated lacey carbon supported copper grid with a grid size of 400 mesh (Merck, Italy) and placing the grids in a closed dish with a drop of water inside the dish so that the evaporation occurs very slowly to reduce the coffee-ring effect. The samples for observing the oligonucleotide coating on GNPs were prepared in lacey carbon coated copper grid to obtain a better background required for visualizing the coating. In the latter case, the samples were drop casted onto a lacey carbon grid supported on a tweezer (image shown in Figure S16, Supporting Information). The particle size distribution of gold nanoparticles was studied by a Litesizer 500 Anton Paar Dynamic Light Scattering (DLS) instrument by placing 1 ml of the sample in a disposable cuvette in the back-scattering mode at an angle of 175°. A Cary 3500 UV–vis spectrophotometer was used for measuring the absorbance of samples. The concentration of as-synthesized GNPs was estimated to be 0.67 nM based on the absorbance at 520 nm and an extinction coefficient of 8.78×10^8 $M^{-1}cm^{-1}$ for 19 nm GNPs.[77]

Association of Oligonucleotides with Gold Nanoparticles: To assess the interaction of oligonucleotides with GNPs, the following conditions were used: pH (3, 6, 9), temperature (4°C, 25°C, -20°C) and salt concentration (1 mM, 10 mM, 30 mM). For sample preparation, the pH of nuclease free water was adjusted to 3, 6, and 9 and the GNPs pellets, obtained by centrifugation at 10,000 rpm for 10 minutes, were resuspended in water at different pH. The pH of water was adjusted by using 0.5 M HCl and 0.5 M NaOH. For the variation of salt concentration, 1mM, 10 mM and 30 mM NaCl solutions were first prepared in water followed by the addition of GNPs pellet as described earlier. The concentration of oligonucleotides in solution was determined through the Beer-Lambert law using the absorbance at 260 nm and extinction coefficients based on the nearest-neighbor rule.[78] Oligonucleotides were added to 1 mL of GNPs at different pH and salt conditions to a final concentration of 5 μM and incubated overnight (16 h). The concentration of gold nanoparticles was kept constant for all the measurements (approximately 0.67 nM). For the temperature control experiments, oligonucleotides were incubated with 1 mL of as-synthesized GNPs at 21 °C, 4 °C, and -20 °C. Bare oligonucleotides and GNPs were also prepared in 1 mL water at different pH, salt concentration, and temperature as control samples.

The extinction spectra were obtained with a Cary 3000 UV–vis spectrophotometer at room temperature in the range of 200–800 nm and a data interval of 1 nm. The measurements were recorded by placing 700 μL of solution in a clean quartz cuvette of 1 cm optical path length. The hydrodynamic diameter obtained by DLS was plotted as a function of relative frequency weighted intensity (%) obtained from three measurements. Note that for the samples at pH 3, it was not possible to obtain a reasonable measurement of particle size distribution by DLS for most of the oligonucleotides due to rapidly changing dynamics of the system inside the cuvette, mostly caused by the aggregation of GNPs. Thus the measurements for pH 6 and 9 was only presented.

Kinetics of Binding of Oligonucleotides to GNPs: A time dependent interaction analysis was conducted to determine how fast the oligonucleotides bind to GNPs. It was observed that the spectral changes due to binding were more rapid in the first hour (>50% ΔI) and then gradually slowed down depending on base composition. To set a standard timeframe of observation for all samples, the time point was chosen at which the changes in spectral intensity were <10% for at least 15 minutes. For most of the samples, this time point was around 60 minutes and thus the UV-vis absorbance spectra were collected from 0–60 min. The resulting complex spectral profiles were processed by Multivariate Curve Resolution Algorithm (MCR),[79] which s a data decomposition method based on Beer's Law generally used for mathematically deconvoluting mixtures of overlapping signals originating from different chemical compounds/phenomena described by the spectra. MCR is conceptually similar to Principal Component Analysis (PCA),[80] and can be seen as a "constrained" version of it. The possibility of constraining the model allows to obtain a pure spectral profile and a vector of relative concentrations (one concentration value for each sample) for each resolved component. The main idea behind MCR is that if the number of modelled components matches the complexity of the system (i.e., its chemical rank), then each modelled component should be interpretable as one chemical compound/phenomenon occurring within the studied system. MCR assumes that each component's spectrum or profile is known, and it aims to find their proportions in the observed data, by applying Beer's Law using a decomposition equation and solving it by the alternating least squares procedure.[79]

In this study, MCR was applied to each individual oligonucleotide spectral dataset, all organized as follows: Each column corresponding to the spectral absorbance at a specific wavelength, and each row corresponding to a measurement done at a specific time point. In this way, the resolved pure concentrations can be interpreted as they evolve over time. For all MCR models the non-negativity constraint was applied to both the concentrations and the profiles, using in both cases the fast non-negative least squares algorithm,[81] with a maximum number of iterations set to 1000. For all datasets the MCR models from 2 to 4 components were built and inspected to determine the chemical rank of the data. The expected 3 chemical components appeared to be well modelled with the corresponding 3-components MCR model in all cases, to the results discussed will mainly be referred to the 3-components models. In the few cases when models with a different number of components provided equally plausible solutions,[82] 4-components models were discussed, based on the chemical knowledge.

The data were pre-processed prior to MCR modelling using the same approach: first, the Standard Normal Variate (SNV),[83] normalization was applied to each spectrum to remove possible scattering effects, then an offset to bring the whole dataset back to positive values was added. The former step was employed to ensure that the non-negativity constraint imposed during MCR modelling could yield interpretable resolved spectral profiles: this was particularly important when modelling spectral data, as both the spectral profiles and the concentrations were expected to be positive, just like the chemical mixtures in the real world. The averaging time of spectra collection was reduced to 0.004 s to capture the maximum number of spectra possible within the detection limits of the instrument over the defined timeframe. As a result of lower averaging time, the MCR curves had to be smoothed to improve the signal quality.

Data Processing and Representation: The spectral shift (nm) and percentage change in intensity (%ΔI) were quantified by dividing the entire spectra (baseline corrected) into two regions: Oligonucleotide (230-300 nm) and GNP (400-800 nm). The %ΔI for each of the conjugated samples were calculated with respect to their bare counterparts. Baseline corrections were done in Origin 8.0 using the user-defined point selection for the baseline. The peak positions (nm) and relative change in absorbance before and after the baseline correction remained unchanged. The error

bars were reported as standard deviation of triplicate measurements, unless otherwise stated.

Supporting Information

Supporting Information is available from the Wiley Online Library or from the author.

Conflict of Interest

The authors declare no conflict of interest.

Data Availability Statement

The data that support the findings of this study are available from the corresponding author upon reasonable request.

[1] B. Liu, J. Liu, *Anal. Methods* **2017**, *9*, 2633.
[2] Y. Ye, S. Hou, X. Wu, X. Cheng, S. He, *Langmuir* **2022**, *38*, 4625.
[3] B. Liu, J. Liu, *Langmuir* **2019**, *35*, 6476.
[4] C. Izanloo, *Nucleosides., Nucleotides Nucleic Acids* **2017**, *36*, 571.
[5] J. J. Storhoff, R. Elghanian, R. C. Mucic, C. A. Mirkin, R. L. Letsinger, *J. Am. Chem. Soc.* **1998**, *120*, 1959.
[6] K. Glynou, P. C. Ioannou, T. K. Christopoulos, V. Syriopoulou, *Anal. Chem.* **2003**, *75*, 4155.
[7] P. Liang, J. Canoura, H. Yu, O. Alkhamis, Y. Xiao, *ACS Appl. Mater. Interfaces* **2018**, *10*, 4233.
[8] C. S. Lee, H. Kim, J. Yu, S. H. Yu, S. Ban, S. Oh, D. Jeong, J. Im, M. J. Baek, T. H. Kim, *Eur. J. Med. Chem.* **2017**, *142*, 416.
[9] S. Dhar, W. L. Daniel, D. A. Giljohann, C. A. Mirkin, S. J. Lippard, *J. Am. Chem. Soc.* **2009**, *131*, 14652.
[10] L. Y. Chou, F. Song, W. C. Chan, *J. Am. Chem. Soc.* **2016**, *138*, 4565.
[11] L. Y. Chou, K. Zagorovsky, W. C. Chan, *Nat. Nanotechnol.* **2014**, *9*, 148.
[12] A. Kumar, M. Pattarkine, M. Bhadbhade, A. B. Mandale, K. N. Ganesh, S. S. Datar, C. V. Dharmadhikari, M. Sastry, *Adv. Mater.* **2001**, *13*, 341.

[13] A. Epanchintseva, P. Vorobjev, D. Pyshnyi, I. Pyshnaya, *Langmuir* **2018**, *34*, 164.
[14] X. Zhang, B. Liu, N. Dave, M. R. Servos, J. Liu, *Langmuir* **2012**, *28*, 17053.
[15] B. Zheng, S. Cheng, W. Liu, M. H. Lam, H. Liang, *Anal. Chim. Acta* **2012**, *741*, 106.
[16] M. P. Kushalkar, B. Liu, J. Liu, *Langmuir* **2020**, *36*, 11183.
[17] B. Liu, J. Liu, *Langmuir* **2019**, *35*, 6476.
[18] Y. Ye, S. Hou, X. Wu, X. Cheng, S. He, *Langmuir* **2022**, *38*, 4625.
[19] M.-Q. He, S. Chen, K. Yao, K. Wang, Y.-L. Yu, J.-H. Wang, *Small Methods* **2019**, *3*, 1900017.
[20] B. Liu, J. Liu, *J. Am. Chem. Soc.* **2017**, *139*, 9471.
[21] B. Liu, Y. Zhao, Y. Jia, J. Liu, *J. Am. Chem. Soc.* **2020**, *142*, 147029.
[22] M. Hu, C. Yuan, T. Tian, X. Wang, J. Sun, E. Xiong, X. Zhou, *J. Am. Chem. Soc.* **2020**, *142*, 7506.
[23] M. Huang, E. Xiong, Y. Wang, M. Hu, H. Yue, T. Tian, D. Zhu, H. Liu, X. Zhou, *Nat. Commun.* **2022**, *13*, 968.
[24] E. M. Nelson, L. J. Rothberg, *Langmuir.* **2011**, *27*, 1770.
[25] S. J. Hurst, A. K. R. Lytton-Jean, C. A. Mirkin, *Anal. Chem.* **2006**, *78*, 8313.
[26] Y. Hao, Y. Li, L. Song, Z. Deng, *J. Am. Chem. Soc.* **2021**, *143*, 3065.
[27] A. Prado, D. González-Rodríguez, Y. L. Wu, *ChemistryOpen* **2020**, *9*, 409.
[28] S. Aoyagi, Y. Inoue, *J. Biol. Chem.* **1968**, *243*, 514.
[29] D. M. Gray, S. H. Hung, K. H. Johnson, in *Methods in Enzymology*, Academic Press, Cambridge, **1995**, Vol. *246*, pp. 19–34.
[30] H. Arafune, A. Yamaguchi, M. Namekawa, Y. Sato, T. Itoh, R. Yoshida, N. Teramae, *Nat. Commun.* **2014**, *5*, 5151.
[31] H. Penázová, M. Vorlickova, *Biophys. J.* **1997**, *73*, 2054.
[32] D. T. Browne, J. Eisinger, N. J. Leonard, *J. Am. Chem. Soc.* **1968**, *90*, 7302.
[33] A. Sarmah, R. K. Roy, *J. Phys. Chem. C* **2015**, *119*, 17940.
[34] L. A. Espinosa Leal, O. Lopez-Acevedo, *Nanotechnol. Rev.* **2015**, *4*, 173.
[35] J. M. Carnerero, A. Sánchez-Coronilla, E. I. Martín, A. Jimenez-Ruiz, R. Prado-Gotor, *Phys. Chem. Chem. Phys.* **2017**, *19*, 44.
[36] G. J. Cao, H. G. Xu, R. Z. Li, W. Zheng, *J. Chem. Phys.* **2012**, *136*, 014305.
[37] T. Yoshimoto, M. Seki, H. Okabe, N. Matsuda, D. Y. Wu, M. Futamata, *Chem. Phys. Lett.* **2022**, *786*, 139202.
[38] M. Bhamidipati, L. Fabris, *Bioconjug. Chem.* **2017**, *28*, 449.
[39] N. Varghese, U. Mogera, A. Govindaraj, A. Das, P. K. Maiti, A. K. Sood, C. N. Rao, *ChemPhysChem* **2009**, *10*, 206.
[40] A. Gourishankar, S. Shukla, K. N. Ganesh, M. Sastry, *J. Am. Chem. Soc.* **2004**, *126*, 13186.
[41] K. M. Guckian, B. A. Schweitzer, R. X. Ren, C. J. Sheils, D. C. Tahmassebi, E. T. Kool, *J. Am. Chem. Soc.* **2000**, *122*, 2213.
[42] A. V. Tataurov, Y. You, R. Owczarzy, *Biophys. Chem.* **2008**, *133*, 66.
[43] T. C. Jenkins, in *Drug-DNA Interaction Protocols*, (Ed.: K. R. Fox), Humana Press, Totowa, NJ **1997**, Vol. *90*, pp. 195–218.
[44] M. Sirajuddin, S. Ali, A. Badshah, *J. Photochem. Photobiol., B* **2013**, *124*, 1.
[45] M. M. Warshaw, I. Jr. Tinoco, *J. Mol. Biol.* **1965**, *13*, 54.
[46] D. Voet, W. B. Gratzer, R. A. Cox, P. Doty, *Biopolym.: Orig. Res. Biomol.* **1963**, *1*, 193.
[47] D. Touboul, G. Bouchoux, R. Zenobi, *J. Phys. Chem. B* **2008**, *112*, 11716.
[48] E. Papadopoulou, S. E. Bell, *J. Phys. Chem. C* **2010**, *114*, 22644.
[49] R. B. Martin, *Acc. Chem. Res.* **1985**, *18*, 32.
[50] S. Benabou, A. Aviñó, R. Eritja, C. González, R. Gargallo, *RSC Adv.* **2014**, *4*, 26956.
[51] B. E. Billinghurst, S. A. Oladepo, G. R. Loppnow, *J. Phys. Chem. B* **2009**, *113*, 7392.

[52] B. Rafique, A. M. Khalid, K. Akhtar, A. Jabbar, *Biosens. Bioelectron.* **2013**, *44*, 21.

[53] A. Garbesi, G. Gottarelli, P. Mariani, G. P. Spada, *Pure Appl. Chem.* **1993**, *65*, 641.

[54] H. Kimura-Suda, D. Y. Petrovykh, M. J. Tarlov, L. J. Whitman, *J. Am. Chem. Soc.* **2003**, *125*, 9014.

[55] M. Deiana, K. Matczyszyn, J. Massin, J. Olesiak-Banska, C. Andraud, M. Samoc, *PLoS One* **2015**, *10*, 0129817.

[56] B. Alberts, A. Johnson, J. Lewis, M. Raff, K. Roberts, P. Walter, *Molecular Biology of the Cell*, Garland Science, New York, USA **2002**, Ch. 4.

[57] R. An, Y. Jia, B. Wan, Y. Zhang, P. Dong, J. Li, X. Liang, *PLoS One* **2014**, *9*, 115950.

[58] H. Kimura-Suda, D. Y. Petrovykh, M. J. Tarlov, L. J. Whitman, *J. Am. Chem. Soc.* **2003**, *125*, 9014

[59] D. L. Nelson, A. L. Lehninger, M. M. Cox, in *Lehninger Principles of Biochemistry*, Macmillan, USA **2008**.

[60] H. Chen, S. P. Meisburger, S. A. Pabit, J. L. Sutton, W. W. Webb, L. Pollack, *Proc. Natl. Acad. Sci. USA* **2012**, *109*, 799.

[61] D. P. Salem, X. Gong, A. T. Liu, V. B. Koman, J. Dong, M. S. Strano, *J. Am. Chem. Soc.* **2017**, *139*, 16791.

[62] J. J. Storhoff, R. Elghanian, C. A. Mirkin, R. L. Letsinger, *Langmuir* **2002**, *18*, 6666.

[63] J. A. Dougan, C. Karlsson, W. E. Smith, D. Graham, *Nucleic Acids Res.* **2007**, *35*, 3668.

[64] J. Liu, *Phys. Chem. Chem. Phys.* **2012**, *14*, 10485

[65] L. Sun, Z. Zhang, S. Wang, J. Zhang, H. Li, L. Ren, J. Weng, Q. Zhang, *Nanoscale Res. Lett.* **2009**, *4*, 216.

[66] J. M. Carnerero, A. Jimenez-Ruiz, P. M. Castillo, R. Prado-Gotor, *ChemPhysChem.* **2017**, *18*, 17.

[67] M. Cárdenas, J. Barauskas, K. Schillén, J. L. Brennan, M. Brust, T. Nylander, *Langmuir* **2006**, *22*, 3294.

[68] J. Liu, *Phys. Chem. Chem. Phys.* **2012**, *14*, 10485.

[69] C.-C. Wang, S.-M. Wu, H.-W. Li, H.-T. Chang, *ChemBioChem* **2016**, *17*, 1052.

[70] Y. C. Shiang, C. C. Huang, T. H. Wang, C. W. Chien, H. T. Chang, *Adv. Funct. Mater.* **2010**, *20*, 3175.

[71] D. Kim, Y. Y. Jeong, S. Jon, *ACS Nano* **2010**, *4*, 3689.

[72] L. Song, V. H. Ho, C. Chen, Z. Yang, D. Liu, R. Chen, D. Zhou, *Adv. Healthcare Mater.* **2013**, *2*, 275.

[73] H. Z. Lai, S. G. Wang, C. Y. Wu, Y. C. Chen, *Anal. Chem.* **2015**, *87*, 2114.

[74] M. P. Girard, S. Osmanov, O. M. Assossou, M. P. Kieny, *Vaccine* **2011**, *29*, 6191.

[75] T. T. Le, B. Adamiak, D. J. Benton, C. J. Johnson, S. Sharma, R. Fenton, J. W. McCauley, M. Iqbal, A. E. G. Cass, *Chem. Commun.* **2011**, *50*, 15533.

[76] B. V. Enustun, J. Turkevich, *J. Am. Chem. Soc.* **1963**, *85*, 3317.

[77] X. Liu, M. Atwater, J. Wang, Q. Huo, *Colloids Surf., B* **2007**, *58*, 3.

[78] A. V. Tataurov, Y. You, R. Owczarzy, *Biophys. Chem.* **2008**, *133*, 66.

[79] A. de Juan, R. Tauler, *Anal. Chim. Acta* **2021**, *1145*, 59.

[80] R. Bro, A. K. Smilde, *Anal. Methods* **2014**, *6*, 2812.

[81] R. Bro, S. De Jong, *J. Chemom.* **1997**, *11*, 393.

[82] A. De Juan, J. Jaumot, R. Tauler, *Anal. Methods* **2014**, *6*, 4964

[83] Å. Rinnan, L. Nørgaard, F. van den Berg, J. Thygesen, R. Bro, S. B. EngelsenS, in *Infrared Spectroscopy for Food Quality Analysis and Control* (Ed.: D.-W. Sun), Elsevier, Amsterdam The Netherlands **2009**, 29–50.